

Diffusion and interactions of interstitials in hard-sphere interstitial solid solutions

Berend van der Meer, Emma Lathouwers, Frank Smalenburg, and Laura Filion

Citation: *The Journal of Chemical Physics* **147**, 234903 (2017); doi: 10.1063/1.5003905

View online: <https://doi.org/10.1063/1.5003905>

View Table of Contents: <http://aip.scitation.org/toc/jcp/147/23>

Published by the [American Institute of Physics](#)

Articles you may be interested in

[Assessment by Monte Carlo computer simulations of the phase behavior of hard spherocylinders confined within cylindrical cavities](#)

The Journal of Chemical Physics **147**, 234902 (2017); 10.1063/1.5017844

[Crystallization of Lennard-Jones liquids under dynamic compression: Heterogeneous and homogeneous nucleation](#)

The Journal of Chemical Physics **147**, 244501 (2017); 10.1063/1.5010088

[Reliability assessment for large-scale molecular dynamics approximations](#)

The Journal of Chemical Physics **147**, 234106 (2017); 10.1063/1.5009431

[Mean field theory of the swap Monte Carlo algorithm](#)

The Journal of Chemical Physics **147**, 234506 (2017); 10.1063/1.5009116

[Aging near rough and smooth boundaries in colloidal glasses](#)

The Journal of Chemical Physics **147**, 224505 (2017); 10.1063/1.5000445

[From properties to materials: An efficient and simple approach](#)

The Journal of Chemical Physics **147**, 234105 (2017); 10.1063/1.5009548

PHYSICS TODAY

WHITEPAPERS

ADVANCED LIGHT CURE ADHESIVES

Take a closer look at what these environmentally friendly adhesive systems can do

READ NOW

PRESENTED BY
 MASTERBOND
ADHESIVES | SEALANTS | COATINGS

Diffusion and interactions of interstitials in hard-sphere interstitial solid solutions

Berend van der Meer,¹ Emma Lathouwers,¹ Frank Smalenburg,² and Laura Filion¹

¹*Soft Condensed Matter, Debye Institute for Nanomaterials Science, Utrecht University, Princetonplein 5, 3584 CC Utrecht, The Netherlands*

²*Institut für Theoretische Physik II: Weiche Materie, Heinrich-Heine-Universität Düsseldorf, Universitätsstr. 1, 40225 Düsseldorf, Germany*

(Received 8 September 2017; accepted 30 November 2017; published online 19 December 2017)

Using computer simulations, we study the dynamics and interactions of interstitial particles in hard-sphere interstitial solid solutions. We calculate the free-energy barriers associated with their diffusion for a range of size ratios and densities. By applying classical transition state theory to these free-energy barriers, we predict the diffusion coefficients, which we find to be in good agreement with diffusion coefficients as measured using event-driven molecular dynamics simulations. These results highlight that transition state theory can capture the interstitial dynamics in the hard-sphere model system. Additionally, we quantify the interactions between the interstitials. We find that, apart from excluded volume interactions, the interstitial-interstitial interactions are almost ideal in our system. Lastly, we show that the interstitial diffusivity can be inferred from the large-particle fluctuations alone, thus providing an empirical relationship between the large-particle fluctuations and the interstitial diffusivity. *Published by AIP Publishing.* <https://doi.org/10.1063/1.5003905>

I. INTRODUCTION

Solid solutions occur when one species is dissolved within the host crystal of another species. The Hume-Rothery rules state that whether or not a solid solution may form, and in which way the two components mix, is largely controlled by the ratio $q = \sigma_a/\sigma_b$ of the diameters $\sigma_{a,b}$ of the two species.¹ In particular, we expect two distinct types of solid solutions to occur depending on the size ratio. More specifically, for $q \gtrsim 0.85$, solid solutions occur where the solute is incorporated into the solvent crystal lattice via substitution, i.e., by replacing a particle in the host lattice, while at smaller size ratios $q \lesssim 0.4$, small solutes are fitted interstitially within the voids of the host crystal lattice.¹ Examples of such solid solutions can be found in the atomic realm but also in colloidal systems.^{2–12}

Over the last decades, colloidal “hard spheres” have provided an excellent model system to investigate a variety of problems in condensed matter physics, such as glass transitions,^{13–15} crystal nucleation,^{16–21} and optimal packings.^{22–25} Likewise, binary mixtures of hard spheres provide a simple model system to study solid solutions. More specifically, theory and simulations reveal a thermodynamically stable substitutionally disordered crystal phase in hard-sphere systems with size ratios $q \geq 0.85$, thus highlighting the validity of the Hume-Rothery rules.^{2–7} Moreover, recent colloidal realizations of interstitial solid solutions have opened the door for the direct observation of these mixtures in real space and real time using microscopy.^{8–10} For hard spheres, both experiments and simulations demonstrate the stability of interstitial solid solutions for binary mixtures with a size ratio of $q = 0.30$.⁸ This interstitial solid solution is obtained by filling the octahedral holes of a face-centered cubic crystal of large particles with small particles. It was shown that the diffusion of the small

particles occurs through hopping between neighbouring octahedral holes via an intermediate tetrahedral hole. Surprisingly, in this system, the interstitial diffusion increased with increasing interstitial concentration, due to a lowering of the free-energy barrier associated with interstitial diffusion.⁸ More recently, Tauber *et al.* found that in body-centered cubic crystals of soft particles, the interstitial dynamics deviate substantially from predictions based on classical transition state theory in which the base crystal was considered to be static.⁹ Such classical theories attempt to predict the interstitial dynamics from the activation barrier associated with an interstitial particle hopping between adjacent interstitial sites.²⁶ The breakdown of transition state theory in Ref. 9 was attributed to the importance of thermal excitations of the host crystal lattice and to the presence of strong interstitial-interstitial interactions. It remains to be seen whether or not transition state theory can capture the interstitial dynamics in the binary hard-sphere model system.

In this paper, we study the dynamics and interactions of interstitials in hard-sphere interstitial solid solutions. We calculate the free-energy barriers associated with interstitial diffusion for a wide range of size ratios and densities. For very small interstitials $q = 0.1$, we find that the barrier height depends only on the density of the large particles and not on the stoichiometry. For interstitials of intermediate size ratios $0.2 \leq q \leq 0.35$, we observe that for increasing stoichiometry, the barrier height decreases. For large interstitials $q > 0.35$, we observe a more intricate dependence of the barrier height on the stoichiometry, where the barrier transitions from decreasing to increasing height with stoichiometry, as the large-sphere density is increased. Next, we apply classical transition state theory to these free-energy barriers in order to predict the diffusion coefficients of interstitials and obtain

good agreement with diffusion coefficients as measured using event-driven molecular dynamics simulations. These results highlight that transition state theory can capture the interstitial dynamics in the hard-sphere model system. Additionally, we quantify the interactions between interstitials in our system and find that, apart from excluded volume interactions, the interstitial-interstitial interactions are almost ideal. Finally, we show that the interstitial diffusivity can be inferred from the large-particle fluctuations alone, thus providing an empirical relationship between the two.

II. METHODS

Using computer simulations, we investigate interstitial solid solutions consisting of N_l large particles and N_s small particles with a size ratio $q = \sigma_s/\sigma_l$, where σ_l and σ_s are the large and small particle diameters, respectively. The stoichiometry is defined as $n = N_s/N_l$. The interstitial solid solutions are initialized by creating a face-centered cubic crystal of large particle and distributing the small interstitials randomly among the octahedral holes. The dynamics of these systems are investigated using event-driven molecular dynamics (EDMD) simulations.^{27,28} We define the EDMD unit time as $\tau = \sqrt{\beta m_l \sigma_l^2}$, where m_l is the mass of a large particle and $\beta = 1/k_B T$ with k_B being Boltzmann's constant and T being the temperature. For the small particle mass, we used $m_s = m_l \sigma_s^3/\sigma_l^3$.

For the calculations of the free-energy barrier associated with interstitial diffusion and the calculations of the interstitial-interstitial interactions, we employ Monte Carlo (MC) simulations. In these MC simulations, the incorporation of ‘‘hopping’’ moves allows for more efficient sampling. More specifically, apart from regular translational moves of particles, we also allow the small particles to move an integer number of lattice spacings, which greatly enhances the probability that an interstitial will jump into another octahedral hole.

In our simulations, we typically fix the packing fraction of the large spheres $\eta_l = \pi N_l \sigma_l^3/6V$, where V is the volume of the system, and vary the stoichiometry. Note that for all analyses, we corrected for drift in the center of mass of the host lattice.

III. RESULTS

A. Diffusion of interstitial particles

1. Free-energy barriers

It has been previously observed in Ref. 8 that in hard-sphere interstitial solid solutions, the small particles reside mainly in the octahedral holes in the host lattice [Fig. 1(a)] and diffuse by hopping through a neighbouring tetrahedral hole [Fig. 1(b)]. It should be noted that each octahedral hole is connected to eight adjacent tetrahedral holes, while each tetrahedral is connected to four octahedral holes. We start off by examining the free-energy barriers associated with the transitions between octahedral and tetrahedral holes, for a range of large-sphere packing fractions η_l , stoichiometries n , and size ratios q . To this end, we project the positions of the

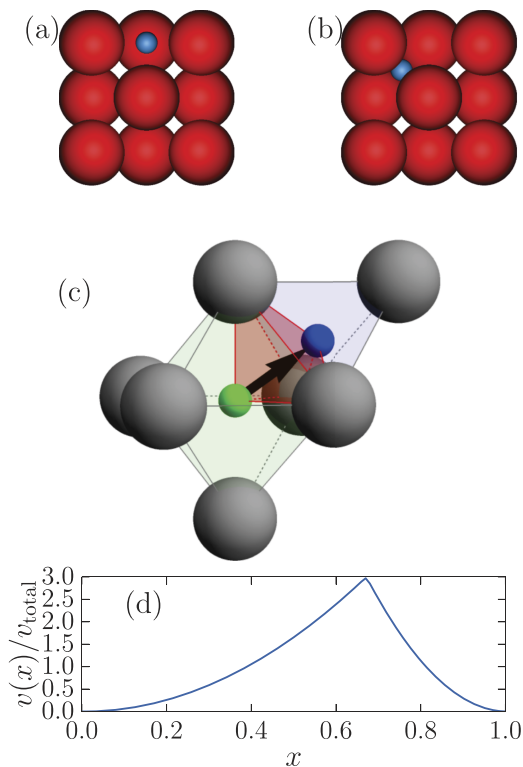


FIG. 1. Interstitial particle (blue) located at (a) an octahedral hole $x = 0$ and (b) a tetrahedral hole $x = 1$. (c) Schematic representation of the volume (red) projected onto the line between a specific octahedral hole (green) and a specific tetrahedral hole (blue). Large particles are indicated in gray. The black arrow indicates the path along which x is measured. (d) The projected volume $v(x)$ along the coordinate x .

interstitial particles onto the line that connects the neighbouring octahedral and tetrahedral holes. We obtain a free-energy barrier using $\beta F(x) = -\ln(P(x)\sigma_l^3/v(x))$ with $P(x)$ being the probability distribution function of the projected particle coordinate x and $v(x)$ being the projected volume, as shown in Figs. 1(c) and 1(d). Hence we normalize this free-energy barrier to the probability distribution function of an ideal gas. Here $x = 0$ corresponds to the particle being located at the octahedral hole, and $x = 1$ corresponds to the tetrahedral hole.

We show these free-energy barriers for a range of size ratios and stoichiometries in Figs. 2 and 3, for host crystal packing fractions of $\eta_l = 0.60$ and $\eta_l = 0.64$, respectively. We observe these free-energy barriers to exhibit a clear single peak around $x = 0.66$. This can be understood from the fact that the channel between the octahedral and tetrahedral holes is narrowest at $x = 2/3$. Hence, intuitively the small particles are least likely to be found at this position. We identify three behaviours of the free-energy barrier as the stoichiometry n is increased, depending on the size ratio q .

For very small interstitials $q = 0.1$, we find that the free-energy barriers are independent of the interstitial concentration [Figs. 2(a) and 3(a)]. Here, the diffusion of small particles is governed entirely by the packing fraction of the host crystal. In other words, the interstitials in these systems behave almost ideally. We therefore expect that these systems provide an excellent starting point for more theoretical investigations of diffusion in such systems.

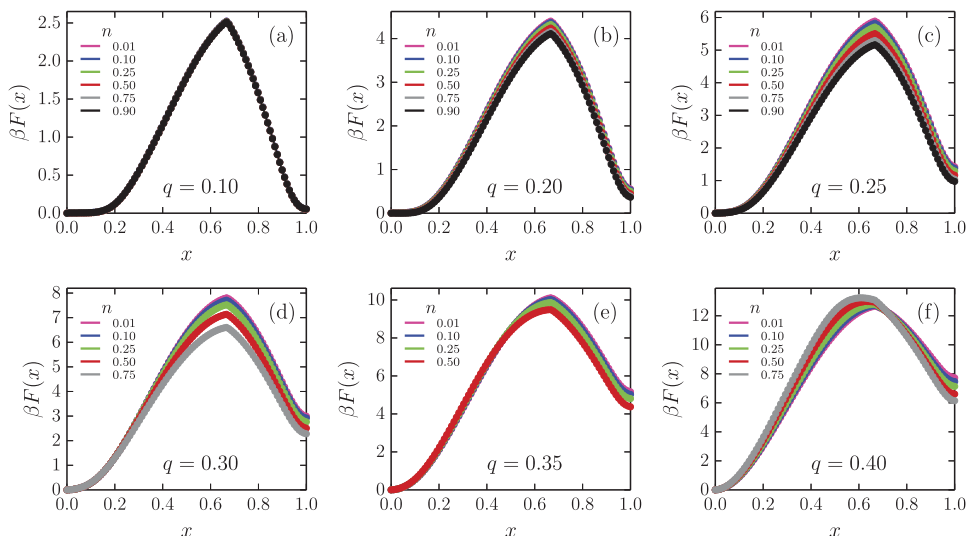


FIG. 2. Free-energy barriers associated with the diffusion of interstitials at a large-sphere packing fraction $\eta_l = 0.60$ for various size ratios: (a) $q = 0.10$, (b) $q = 0.20$, (c) $q = 0.25$, (d) $q = 0.30$, (e) $q = 0.35$, and (f) $q = 0.40$.

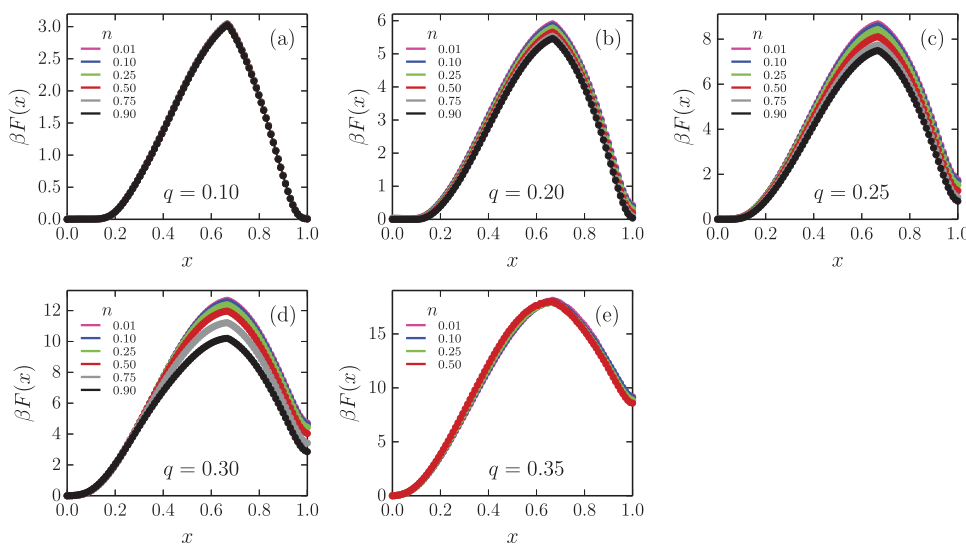


FIG. 3. Free-energy barriers associated with the diffusion of interstitials at a large-sphere packing fraction $\eta_l = 0.64$ for various size ratios: (a) $q = 0.10$, (b) $q = 0.20$, (c) $q = 0.25$, (d) $q = 0.30$, and (e) $q = 0.35$.

For interstitials of intermediate size ratio $0.2 \lesssim q \lesssim 0.35$, we observe that for increasing stoichiometry n , the free-energy barriers decrease, meaning that diffusion will increase [Figs. 2(b)–2(e) and 3(b)–3(d)]. This is in agreement with Ref. 8, where for a size ratio of $q = 0.30$, the interstitial diffusion was found to increase with increasing stoichiometry. Here we thus show that this feature of increased interstitial diffusivity occurs for a broad range of size ratios.

For large interstitials $q \gtrsim 0.35$, we observe a more intricate dependence of the barrier height on the stoichiometry n . Namely, here we find that the large-sphere density starts to play an important role as well. More specifically, we find that

the barrier transitions from decreasing to increasing height with stoichiometry n , as the large-sphere density is increased. To illustrate this transition, we plot the free-energy barriers for $q = 0.38$ at different large-sphere packing fractions and stoichiometries in Fig. 4. Here, for a large-sphere packing fraction of $\eta_l = 0.60$, we observe that the free-energy barrier goes down with increasing stoichiometry, while at the crossover $\eta_l = 0.61$, the free-energy barriers remain constant, and at $\eta_l = 0.62$, the free-energy barriers increase by increasing the stoichiometry. Note that for very large interstitials $q = 0.40$, the free-energy barriers always increase with increasing stoichiometry n ; see, for example, Fig. 2(f). Interestingly, for these

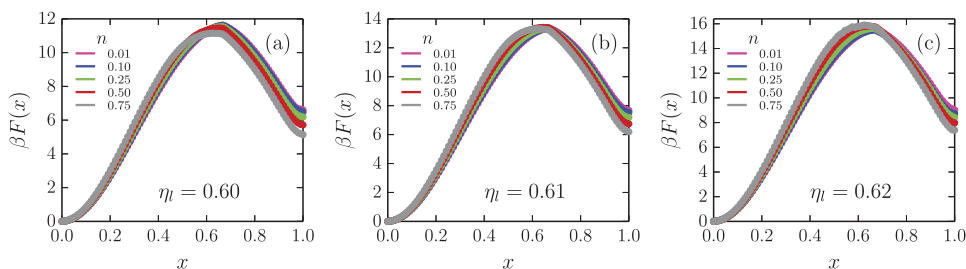


FIG. 4. Free-energy barriers associated with the diffusion of interstitials for a size ratio $q = 0.38$: (a) $\eta_l = 0.60$, (b) $\eta_l = 0.61$, and (c) $\eta_l = 0.62$.

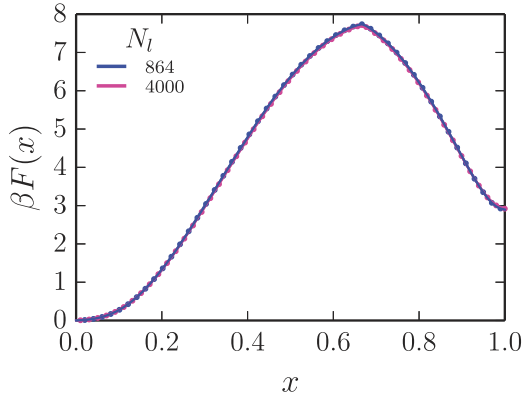


FIG. 5. System-size dependence of the free-energy barriers associated with the diffusion of interstitials for a size ratio $q = 0.30$ at a large-sphere packing fraction $\eta_l = 0.60$ and stoichiometry of $n = 0.10$. The perfect agreement between the two system sizes, $N_l = 864$ and $N_l = 4000$, shows that there are no significant finite-size effects on the free-energy barrier.

large interstitials, we also observe a shift in the peak of the barrier to lower x as the concentration of small particles increases. This effect is stronger at higher packing fraction. This is likely a result of the small particles disturbing the crystal structure of the large particles.

Lastly, we have checked that these free-energy barriers remain constant upon changing the system size. More specifically, we have calculated the free-energy barrier for two different system sizes, namely, $N_l = 864$ and $N_l = 4000$. In Fig. 5, we plot the free-energy barriers at these two different system sizes and find them to agree very well. Clearly, we observe no significant finite-size effects on the free-energy barrier.

2. Mean square displacement of interstitials

Let us now quantify the interstitial diffusivity, in order to be able to compare to predictions based on classical transition state theory in Sec. III A 3. Using EDMD simulations, we study the dynamics of the interstitials by calculating the mean square displacement $\langle \Delta r_s^2(t) \rangle$. While the mean square displacement may exhibit more complex scaling at short and intermediate time scales, we can always safely extract the diffusion coefficient D_s using the long-term diffusive behaviour of the mean square displacement $\langle \Delta r_s^2(t) \rangle$, i.e.,

$$D_s = \lim_{t \rightarrow \infty} \frac{\langle \Delta r_s^2(t) \rangle}{6t}. \quad (1)$$

To illustrate this, we show several mean square displacement curves for different size ratios in Fig. 6. At short time scales, the interstitial particles move ballistically with $\langle \Delta r_s^2(t) \rangle \sim t^2$, while at intermediate time scales, the particle dynamics enter a sub-diffusive regime $\langle \Delta r_s^2(t) \rangle \sim t^\beta$, with $0 \leq \beta < 1$. These sub-diffusive dynamics originate from the interstitial particle being ‘‘caged’’ inside an interstitial hole. Yet, at long time scales, the interstitial particles manage to hop between neighbouring interstitial holes, giving rise to diffusive dynamics, as characterized by $\langle \Delta r_s^2(t) \rangle \sim t$. Using mean square displacements like these, we can extract the interstitial diffusivity for a wide range of large-sphere packing fractions η_l and stoichiometries n .

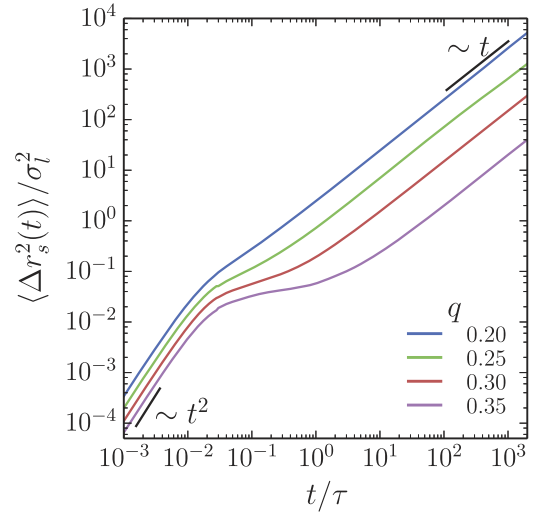


FIG. 6. Mean square displacements of interstitials $\langle \Delta r_s^2(t) \rangle$ for different size ratios q at a large-sphere packing fraction $\eta_l = 0.60$ and a stoichiometry $n = 0.10$.

3. Transition state theory

We now investigate in more detail the relationship between the interstitial diffusivity and the associated free-energy barriers. To this end, we employ transition state theory to calculate the rate associated with an interstitial hopping between octahedral holes. Note that in a face-centered cubic lattice, the octahedral holes are also on a face-centered cubic lattice and that all hopping processes involve an intermediate tetrahedral hole.

In this framework, the diffusion constant of the interstitials D_s^{TST} is given by

$$D_s^{\text{TST}} = \frac{1}{12} k_{oo}^{\text{TST}} a^2, \quad (2)$$

with k_{oo}^{TST} being the rate of hopping between octahedral holes and a being the lattice spacing.²⁹ Following Ref. 30, we calculate the escape rate associated with interstitial hopping from an octahedral hole into a tetrahedral hole using

$$k_{ot}^{\text{TST}} = \frac{D_0}{\int_a^c dx \exp(-\beta V(x)) \int_b^d dy \exp(\beta V(y))}, \quad (3)$$

with D_0 being the short-time diffusion coefficient of the interstitial, $\beta V(x) = -\ln(P(x))$ being the bare free-energy barrier, which in contrast to $\beta F(x)$ has not been normalized to an ideal gas, and the integration limits as indicated in Fig. 7(a). Once an interstitial has jumped into the tetrahedral hole, it can jump to any of four neighbouring octahedral holes, one of which corresponds to its previous position. If we assume this choice to be random, we expect that three out of four hopping events will result in the particle ending up in a different octahedral hole. Note that as the free-energy barriers associated with the first octahedral-to-tetrahedral hopping process are much higher than those associated with the subsequent tetrahedral-to-octahedral hopping process, we expect the rate to be dominated by the first process and make the

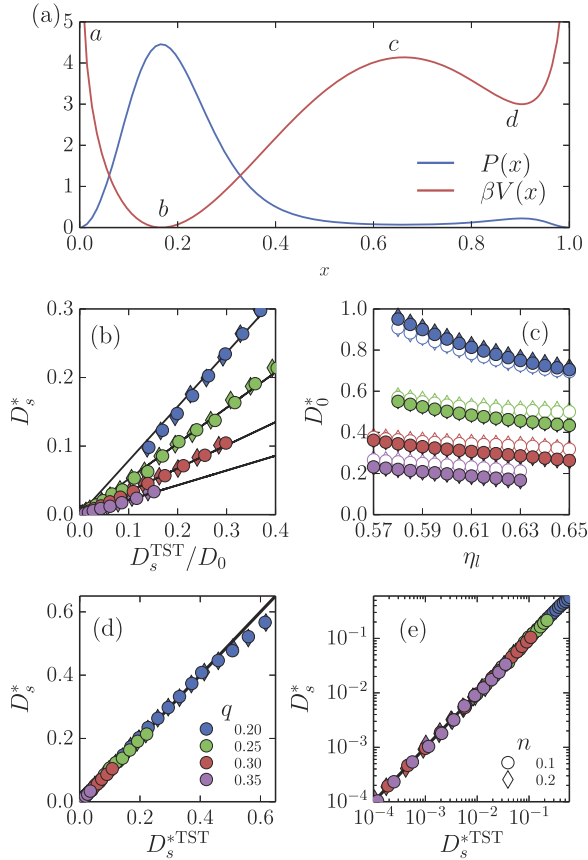


FIG. 7. Predicted and observed diffusion coefficients for interstitials. (a) Sketch of the free-energy barrier $\beta V(x)$ and probability distribution function $P(x)$ as a function of the coordinate x along a transition path. The wells at $x = b$ and $x = d$ correspond to the octahedral and tetrahedral hole, respectively, while $x = c$ corresponds to the transition state. (b) The ratio of the predicted diffusion constant and the short-time diffusion coefficient D_s^{TST}/D_0 versus the measured diffusion coefficient D_s . Black lines correspond to linear fits. (c) The short-time diffusion coefficient as calculated using Eq. (6) (solid markers), and as obtained from the first-order Enskog expression (open markers). (d) The predicted diffusion coefficient D_s^{TST} versus the measured diffusion coefficient D_s . All data collapse onto the black line $D_s^{\text{TST}} = D_s$, showing that the diffusion coefficients can be accurately predicted. (e) Same as in (d) but now on log-log scale. Markers with different colors in (b)–(e) correspond to different size ratios as labeled in (d). Markers with different shapes in (b)–(e) correspond to different stoichiometries as labeled in (e). Diffusion constants were rendered dimensionless using $D^* = D\tau\sigma_l^{-2}$.

approximation

$$k_{oo}^{\text{TST}} \approx \frac{3}{4} k_{ot}^{\text{TST}}, \quad (4)$$

where the prefactor accounts for the possibility of the interstitial hopping back to its original octahedral hole. Hence, we can predict the relative small-particle diffusion constant

$$\frac{D_s^{\text{TST}}}{D_0} \approx \frac{3a^2}{48} \left[\int_a^c dx \exp(-\beta V(x)) \int_b^d dy \exp(\beta V(y)) \right]^{-1}, \quad (5)$$

which can be calculated directly from the measured free-energy barriers. In Fig. 7(b), we compare this quantity to the diffusion constant D_s measured in EDMD simulations. For each size ratio we find an approximately linear relation between D_s^{TST}/D_0 and D_s , as one would expect if D_0 is approximately constant for each size ratio. Note that Fig. 7 includes

data for a wide range of host lattice packing fractions at distinct size ratios (colors), and stoichiometries (symbol shapes).

In order to quantitatively predict the diffusion of the small particles from Eq. (5), we require knowledge of D_0 . In our EDMD simulations, the particles move ballistically at short time scales, and hence D_0 is not clearly defined. Nonetheless, we expect Eq. (3) to hold with an effective D_0 , which is related to the rate of escape attempts from the octahedral hole. Hence, we estimate the effective D_0 by calculating the collision rate of the small particles k_c and use the mean squared displacement to estimate an approximate value for the short-time diffusion coefficient

$$D_0 \approx \frac{\langle \Delta r_c^2 \rangle}{6\tau_c}, \quad (6)$$

with $\langle \Delta r_c^2 \rangle$ being the mean squared displacement between collisions and $\tau_c = 1/k_c$ the time scale between collisions. Note that this corresponds to the diffusion coefficient associated with a three-dimensional random walk with step size $\langle \Delta r_c^2 \rangle^{1/2}$ and time step τ_c .

In Fig. 7(c), we plot D_0 for different size ratios q as a function of the large-sphere packing fraction (solid markers). As expected, D_0 is primarily set by the size (mass) ratio. Additionally, we find that D_0 is mildly dependent on the large-sphere packing fraction and the stoichiometry. These data agree well with a first-order Enskog expression for the self-diffusion coefficient (open markers) given by

$$D_E \approx k_B T \left[\frac{16\pi}{3} \sigma_{ls}^2 \rho_l g_{ls}(\sigma_{ls}) \sqrt{\frac{k_B T \mu_{ls}}{2\pi}} \right]^{-1}, \quad (7)$$

where $\sigma_{ls} = (\sigma_l + \sigma_s)/2$ is the contact diameter, ρ_l is the large-particle number density, $g_{ls}(\sigma_{ls})$ is the value of the pair distribution function at contact, and $\mu_{ls} = (m_l m_s)/(m_l + m_s)$ is the reduced mass.³¹ This expression is expected to work for a binary gas of ballistically moving particles. Nonetheless, it here functions as a simple estimate for the short-time diffusion within the octahedral cages.

Using the short-time diffusion coefficient D_0 as calculated from Eq. (6), we now plot the predicted diffusion coefficient D_s^{TST} versus the measured diffusion coefficient D_s in Figs. 7(d) and 7(e). These data cover a wide range of packing fractions of the host crystal and size ratios, allowing us to test our predicted diffusion constants over multiple orders of magnitude. We find that the diffusion coefficients as predicted from the free-energy barriers D_s^{TST} are in excellent quantitative agreement with the measured diffusion coefficients D_s . Namely, all data largely collapse onto the black line $D_s^{\text{TST}} = D_s$, highlighting that the diffusion coefficients can be accurately predicted. A mild deviation was only observed at very high diffusion constants. This can likely be attributed to the finite time it takes an interstitial to move back from a tetrahedral to an octahedral hole, which is neglected due to our approximation in Eq. (4). Nonetheless, the extremely good overall agreement validates our approximations.

We have thus shown that the diffusion of interstitials in the hard-sphere model system can be accurately described by transition state theory. Interestingly, it was recently found that in soft body-centered cubic crystals the interstitial dynamics deviate substantially from predictions based on classical

transition state theory in which the base crystal was considered to be static.⁹ This breakdown was attributed both to the importance of thermal excitations of the host crystal lattice and to the presence of strong interstitial-interstitial interactions.^{9,11} As such, our data raise the interesting question whether or not such interactions between interstitial particles also play an important role in our system. Thus we will now explore further the interstitial-interstitial interactions in our system.

B. Interactions between interstitials

We evaluate the effective interstitial-interstitial interactions using methods similar to those presented in Refs. 32 and 33. More specifically, we first assign all interstitials to their nearest octahedral hole. Subsequently, for each interstitial pair, we calculate the (discrete) separation distance between the two occupied holes located at positions \mathbf{R}_i and \mathbf{R}_j , which is given by $r = |\mathbf{R}_i - \mathbf{R}_j|$. Using this separation distance r , we define an effective potential between interstitials as

$$\beta U_{\text{eff}}(r) = -\ln \frac{P_{\text{pair}}(r)}{h(r)}, \quad (8)$$

where $P_{\text{pair}}(r)$ is the probability to find two interstitials at a separation distance r and $h(r)$ is the number of octahedral holes at a distance r from a reference octahedral hole.

In Figs. 8(a)–8(d), we plot the effective interactions between interstitials for a range of size ratios q at different stoichiometries n and large-sphere packing fractions η_l . Surprisingly, we find that the interstitials hardly interact with each other. Namely, even for the first shell of neighbouring octahedral sites, we find $\beta U_{\text{eff}} \approx 0$. These ideal interactions are in stark contrast to the strong attractions between self-interstitials in single-component hard spheres.³⁴ Only when the interstitials are assigned to the same octahedral site we observe substantial repulsions between interstitials. This

repulsion arises from the hard-core excluded volume interactions between the particles. Note that for the largest size ratio $q = 0.40$, these excluded volume interactions become so strongly repulsive that we were unable to sample the interactions at $r = 0$.

In order to examine the possibility of interactions between particles in adjacent octahedral and tetrahedral holes, we now compare the spatial distribution of interstitials around an empty octahedral hole to that around an octahedral hole containing an interstitial. If there are attractions (repulsions) present between the interstitials, the local density of interstitials around the filled octahedral hole should be on average higher (lower) than in the case of the empty octahedral hole. We quantify this using a filling parameter defined as

$$f(r) = \frac{\langle N_s(r) \rangle}{h(r)}, \quad (9)$$

with $\langle N_s(r) \rangle$ being the average number of interstitials in a octahedral or tetrahedral hole at a distance r from the reference octahedral hole. In Figs. 8(e)–8(h), we plot this filling parameter associated with the local density of interstitials around the empty octahedral hole and around the filled octahedral hole, using open and solid markers, respectively. Here, two distinct filling fractions are visible, namely, the higher filling fraction occurring at distances corresponding to octahedral holes and a lower filling fraction at distances corresponding to tetrahedral holes. Clearly, we observe that the spatial distribution of interstitials around an empty octahedral hole and around a filled octahedral hole collapses almost perfectly on top of each other (open and solid markers). In both cases, we find the filling fraction of the octahedral and tetrahedral holes to be constant and equal to nf_o and $n(1 - f_o)$, respectively, with f_o being the fraction of interstitials located in octahedral holes. Hence, this further demonstrates that, apart from excluded volume interactions, the interstitial-interstitial interactions are essentially ideal in our system.

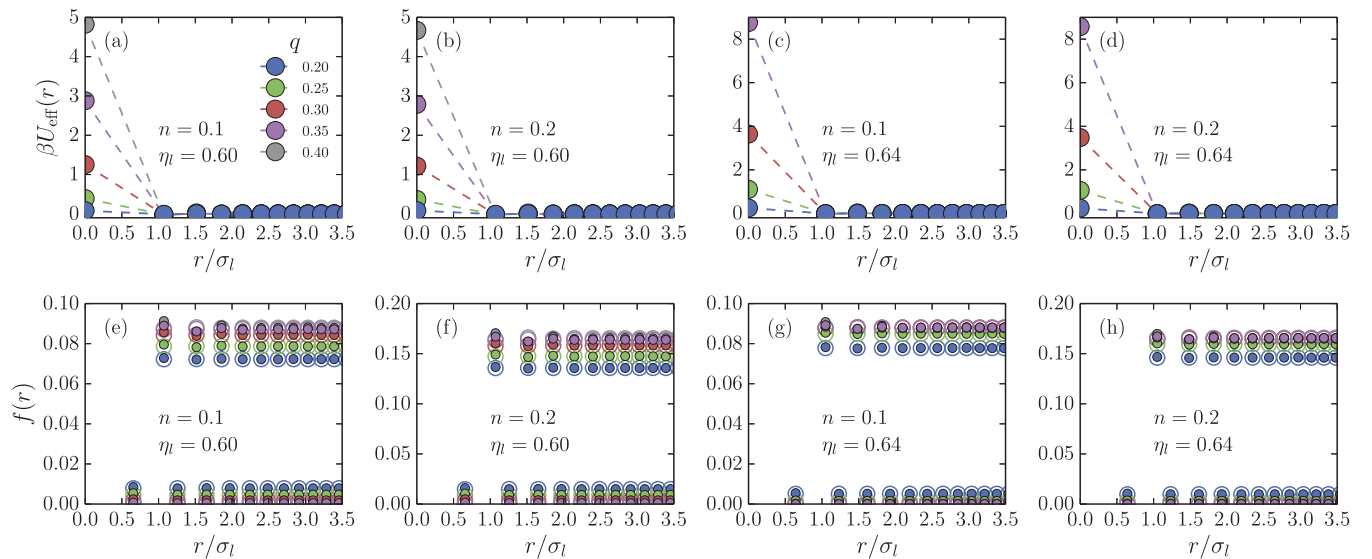


FIG. 8. [(a)–(d)] Effective potential between interstitials $\beta U_{\text{eff}}(r)$ for a range of size ratios q at different stoichiometries n and large-sphere packing fractions η_l . Dashed lines are a guide to the eye. [(e)–(h)] Corresponding filling parameter $f(r)$ around an occupied octahedral hole (solid markers) and around an empty octahedral hole (open markers).

C. Empirical relationship between the large-particle fluctuations and interstitial diffusivity

In Ref. 8, the increase in interstitial diffusivity with increasing stoichiometry n was found to coincide with the increase in displacements of the large particles from their lattice site. Here we quantify further the relationship between the displacements of the particles of the host lattice and the diffusivity of the interstitials. To this end, we define a large-particle fluctuation parameter,

$$\delta_l = \sqrt{\langle |\mathbf{R}_0 - \mathbf{r}_i|^2 \rangle}, \quad (10)$$

with \mathbf{r}_i being the position of a large particle i and \mathbf{R}_0 being the position of the lattice site it occupies. In Fig. 9, we plot the large-particle fluctuation parameter δ_l versus the diffusion constant of the small particles D_s as measured using EDMD simulations. These data were obtained for a wide range of host lattice packing fractions at distinct size ratios (colors) and stoichiometries (symbol shapes). Interestingly, we find that at a fixed size ratio q , these data collapse onto a single curve for a wide range of stoichiometries n . Hence, we conclude that the small particle diffusion in these systems is primarily set by fluctuations of the large particles δ_l . Note that δ_l is dependent not only on the packing fraction of the large particles but also on the number of small particles in the crystal. Hence, a larger concentration of small particles increases the fluctuations of the large particles, which in turn increases the small-particle diffusion. Interestingly, although this is a collective dynamic effect between the small particles,

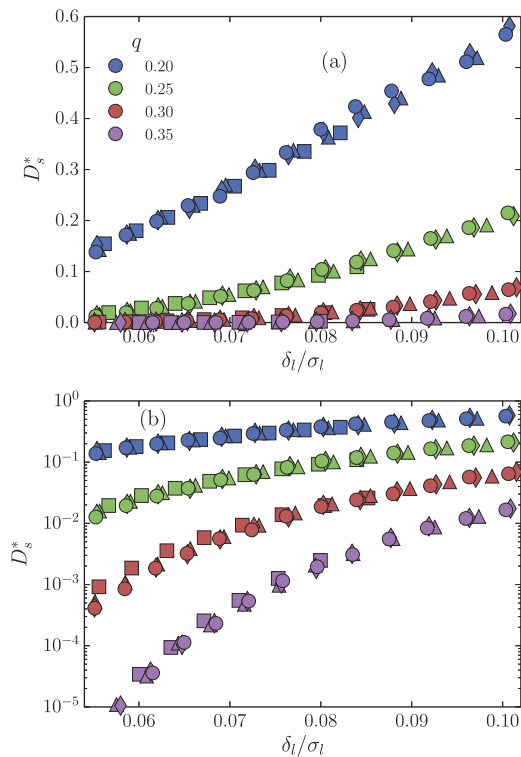


FIG. 9. (a) Relationship between the large-particle fluctuations δ_l and the interstitial diffusivity D_s . (b) Same as in (a) but now on log-log scale. The circle, diamond, triangle, and square markers correspond to stoichiometries of $n=0.1$, $n=0.1875$, $n=0.375$, and $n=0.75$, respectively. Diffusion constants were rendered dimensionless using $D^* = D\tau\sigma_l^{-2}$.

their diffusion is still mainly determined by the large-particle fluctuations.

We would like to highlight that the interstitial diffusivity can thus be inferred from the large-particle fluctuations, assuming the curve has been mapped out for a single interstitial concentration. This could be useful for experiments, in which it is typically easier to track the (relatively static) large particles than the highly diffusive interstitials. Curves like those plotted in Fig. 9 show that the interstitial diffusivity D_s can be estimated quite accurately via δ_l . As such, in experiments, the interstitial diffusivity could be obtained at very low stoichiometry, where it may be possible to track individual interstitials and then may be easily extended to higher concentrations simply by examining the fluctuations of the larger particles.

IV. DISCUSSION AND CONCLUSIONS

In conclusion, we have studied the diffusion and interactions of interstitials in hard-sphere interstitial solid solutions. We have calculated the free-energy barriers associated with interstitial diffusion for a range of size ratios and densities. For very small interstitials $q \lesssim 0.1$, we found that the barrier height depends only on the density of the large particles and does not depend on the stoichiometry n . For interstitials of intermediate size ratio $0.2 \lesssim q \lesssim 0.35$, we observed that for increasing stoichiometry n , the barrier height decreases. For large interstitials $q \gtrsim 0.35$, we observe a more intricate dependence of the barrier height on the stoichiometry n , where the barrier transitions from decreasing to increasing height with stoichiometry, as the large-sphere density is increased. Next, we applied classical transition state theory to these free-energy barriers to predict the diffusion coefficients of interstitials and obtained good agreement with diffusion coefficients as measured using EDMD simulations. Additionally, we have quantified the interactions between interstitials. Apart from excluded volume interactions when two interstitials occupy the same hole, we found these interactions to be almost ideal in our system. Lastly, we showed that the interstitial diffusivity can be inferred from the large-particle fluctuations alone, thus providing an empirical relationship between the large-particle fluctuations and the interstitial diffusivity.

Importantly, we have shown that transition state theory can capture the interstitial dynamics in the hard-sphere model system. The free-energy barriers we used for our calculations were measured in a system where the large particles are fluctuating around their lattice sites. This is in contrast to the predictions made in Ref. 9 in which the base crystal was considered to be static, resulting in the interstitial dynamics deviating substantially from predictions based on classical transition state theory. Our results thus highlight the importance of taking these fluctuations into account in order to obtain the relevant free-energy barrier associated with interstitial diffusion. It would be interesting to see whether incorporating these lattice fluctuations for soft systems can recover an accurate description of the interstitial dynamics using transition state theory.

ACKNOWLEDGMENTS

We acknowledge funding from the Dutch Sector Plan Physics and Chemistry and funding from a NWO-Veni Grant (NWO-VENI Grant No. 680.47.432). We would like to thank Vasileios Prymidis for carefully reading the manuscript.

- ¹W. Hume-Rothery, *The Structures of Alloys of Iron: An Elementary Introduction* (Elsevier, Amsterdam, 2013).
- ²J. Barrat, M. Baus, and J. P. Hansen, *J. Phys. C: Solid State Phys.* **20**, 1413 (1987).
- ³D. A. Kofke, *Mol. Simul.* **7**, 285 (1991).
- ⁴X. Cottin and P. Monson, *J. Chem. Phys.* **99**, 8914 (1993).
- ⁵W. Kranendonk and D. Frenkel, *Mol. Phys.* **72**, 679 (1991).
- ⁶W. Kranendonk and D. Frenkel, *J. Phys.: Condens. Matter* **1**, 7735 (1989).
- ⁷W. Kranendonk and D. Frenkel, *Mol. Phys.* **72**, 699 (1991).
- ⁸L. Filion *et al.*, *Phys. Rev. Lett.* **107**, 168302 (2011).
- ⁹J. Tauber, R. Higler, and J. Sprakel, *Proc. Natl. Acad. Sci. U. S. A.* **113**, 13660 (2016).
- ¹⁰I. R. de Anda, F. Turci, R. Sear, and C. P. Royall, *J. Chem. Phys.* **147**, 124504 (2017).
- ¹¹R. Higler and J. Sprakel, *Sci. Rep.* **7**, 12634 (2017).
- ¹²F. A. Lavergne, S. Diana, D. G. Aarts, and R. P. Dullens, *Langmuir* **32**, 12716 (2016).
- ¹³A. van Blaaderen and P. Wiltzius, *Science* **270**, 1177 (1995).
- ¹⁴E. R. Weeks *et al.*, *Science* **287**, 627 (2000).
- ¹⁵W. K. Kegel and A. van Blaaderen, *Science* **287**, 290 (2000).
- ¹⁶U. Gasser *et al.*, *Science* **292**, 258 (2001).
- ¹⁷S. Auer and D. Frenkel, *Nature* **409**, 1020 (2001).
- ¹⁸S. Auer and D. Frenkel, *Phys. Rev. Lett.* **91**, 015703 (2003).
- ¹⁹A. Cacciuto, S. Auer, and D. Frenkel, *Nature* **428**, 404 (2004).
- ²⁰V. de Villeneuve *et al.*, *J. Phys.: Condens. Matter* **17**, S3371 (2005).
- ²¹E. Allahyarov, K. Sandomirski, S. Egelhaaf, and H. Löwen, *Nat. Commun.* **6**, 7110 (2015).
- ²²L. Filion and M. Dijkstra, *Phys. Rev. E* **79**, 046714 (2009).
- ²³J. K. Kummerfeld, T. S. Hudson, and P. Harrowell, *J. Phys. Chem. B* **112**, 10773 (2008).
- ²⁴P. I. O'Toole and T. S. Hudson, *J. Phys. Chem. C* **115**, 19037 (2011).
- ²⁵A. B. Hopkins, Y. Jiao, F. H. Stillinger, and S. Torquato, *Phys. Rev. Lett.* **107**, 125501 (2011).
- ²⁶C. Wert, *Phys. Rev.* **79**, 601 (1950).
- ²⁷D. C. Rapaport *et al.*, *Comput. Phys.* **10**, 456 (1996).
- ²⁸B. J. Alder and T. E. Wainwright, *J. Chem. Phys.* **31**, 459 (1959).
- ²⁹C. Wert and C. Zener, *Phys. Rev.* **76**, 1169 (1949).
- ³⁰M. Plischke and B. Bergersen, *Equilibrium Statistical Physics* (World Scientific Publishing Co, Inc., Singapore, 1994).
- ³¹H. A. Al-Chalabi and E. McLaughlin, *Mol. Phys.* **19**, 703 (1970).
- ³²W. Lechner and C. Dellago, *Soft Matter* **5**, 2752 (2009).
- ³³W. Lechner, F. Cinti, and G. Pupillo, *Phys. Rev. A* **92**, 053625 (2015).
- ³⁴B. van der Meer, M. Dijkstra, and L. Filion, *J. Chem. Phys.* **146**, 244905 (2017).